Enhanced Wear Resistance and Microstructure of Hypoeutectoid Fe-Cr-C-Nb Alloys via Submerged Arc Surfacing

Ziyi Li[a], Zhongxue Feng[a,c]* , Min Chen[b], Guangyu Zhang[a], Jianwei Chen[a], Boer Cao[a],

Xuefeng Zhang[c], Caiju Li[a], Jianhong Yi[a]

[a]*Kunming University of Science and Technology, Faculty of Materials Science and Engineering, 650093, Kunming, China.*
[b]*Panzhihua University, 617000, Panzhihua, China.*
[c]*Sichuan Vanadium &Titanium Industrial Technology Institute, 617000, Panzhihua, China.*

The Fe-8.2wt.%Cr-0.6wt.%C-Xwt.%Nb surfacing alloys were successfully applied to the substrate of 60CrMnMo steel through the submerged arc surfacing process utilizing a flux-cored welding wire. This study systematically explores the influence of niobium content on the microstructure and properties of these alloys, and delves into the underlying mechanisms. The results show that the microstructure of the surfacing alloy is mainly composed of γ-Fe, α'-Fe, NbC, and Fe-Cr phases. As the niobium content in the surfacing alloy was increased from 0.06% to 4%, the morphology of NbC transitioned from dispersed particles within the matrix to short rod-like structures concentrated at grain boundaries, accompanied by a refinement of the martensite structure. The hardness of the surfacing alloy exhibited an increase of 28%, while its wear rate was halved, resulting in a twofold enhancement in wear resistance. Under identical wear conditions, the wear rate of the experimental 60CrMnMo steel plate was found to be 125 times greater than that of the 4 wt.% Nb surfacing alloy, indicating a significant improvement in wear resistance for this latter alloy. This improvement can be attributed to the rich presence of rod-like NbC in the 4 wt.% Nb surfacing alloy, which is deeply embedded in the martensite matrix and effectively enhances the material, thereby jointly improving overall wear resistance.

Keywords: *submerged arc surfacing, microstructure, hardness, wear resistance, NbC.*

1. Introduction

The failure of parts is inevitable in industrial production as their service time increases[1,2]. The predominant cause of workpiece failure is wear[3,4]. The occurrence of wear not only significantly impacts the precision, performance, and service life of the workpiece but also compromises its reliability and safety, while simultaneously exacerbating material loss. This is highly detrimental to industrial development. The submerged arc surfacing technology is widely utilized in the industry to address this issue, as it not only enhances the wear resistance of parts' surfaces with wear-resistant alloys but also facilitates the repair of parts' surfaces using such alloys. This approach boasts advantages including cost-effective repairs, high efficiency, prolonged service life, and reduced maintenance costs for equipment[5,6]. Consequently, it finds extensive applications in fields like iron and steel manufacturing, metallurgy, mining operations, agricultural machinery production, and petrochemical industries. Therefore, there is a great demand for wear-resistant materials for submerged arc surfacing welding in industry.

The high-chromium eutectic Fe-Cr-C alloy system is widely recognized as the most extensively utilized wear-resistant alloy[7], due to its remarkable wear resistance,

corrosion resistance, and high hardness, primarily attributed to the substantial volume fraction of carbide precipitation ($M_{23}C_6$ and M_7C_3)[8-13]. However, the size of $M_{23}C_6$ and M_7C_3 carbides is considerable, leading to poor binding performance between these larger carbides and the matrix. During service, these oversized $M_{23}C_6$ and M_7C_3 carbides are prone to detach from the matrix, exacerbating wear on the particles and resulting in severe workpiece damage. Consequently, this significantly reduces the lifespan of components, thereby limiting its extensive application[12,14]. In order to minimize the dimensions of $M_{23}C_6$ and M_7C_3 carbides while enhancing their interfacial bonding with the matrix, extensive research has been conducted by researchers. Among various elements, niobium (Nb) is commonly employed to refine the morphology and size of carbides in cast iron, thereby improving its wear resistance[15-23].

However, the conventional high-chromium Fe-Cr-C alloy exhibits elevated carbon content, high hardenability, and poor weldability, rendering it susceptible to cracking during welding[24-26]. Furthermore, despite the refinement of their sizes through the addition of Nb, the primary wear-resistant phases in traditional high-chromium Fe-Cr-C alloys remain $M_{23}C_6$ and M_7C_3. These carbides are still prone to flaking off easily, and when these peeled hard carbides come into

contact with the matrix as wear particles during subsequent wear processes, they exacerbate alloy wear[27-31]. Furthermore, micro-cracks may also develop in proximity to spalling pits, further undermining the alloy's resistance to wear. The Fe-Cr-C surfacing alloys characterized by a substantial presence of $M_{23}C_6$ and M_7C_3 have been thoroughly investigated; however, there is a paucity of literature concerning low and medium carbon Fe-Cr-C surfacing alloys. When Zhao et al.[32] investigated the impact of NbC on the wear resistance of iron-based composite coatings with varying carbon content, they observed that the coating containing 1.4 wt.% C not only exhibited significant granular NbC but also a substantial amount of coarse Cr_7C_3, which contributed to spalling and consequently diminished the overall wear resistance of the coating. Interestingly, no bulky Cr_7C_3 was detected in the coating containing 0.4 wt.% C, while the granular NbC transformed into smaller rod-like structures. Furthermore, no spalling phenomena were observed during wear testing, thereby presenting a novel perspective for investigating a new generation of wear-resistant alloys. Furthermore, in terms of cost-effectiveness, it is recommended to limit the addition of niobium; Jia Hua et al.[33] demonstrated that incorporating 4 wt.% Nb into Fe-Cr-C surfacing alloys yielded optimal hardness and wear resistance.

The primary objective of this study was to fabricate Fe-8.2wt.%Cr-0.6wt.%C-Xwt.%Nb surfacing alloys on the surface of 60CrMoMn steel using a flux-cored welding wire, followed by an investigation into their microstructure and wear resistance properties, as well as the influence of Nb content on these characteristics. Finally, the wear mechanism of Fe-8.2wt.%Cr-0.6wt.%C-Xwt.%Nb surfacing alloys at room temperature is elucidated.

2. Experimental Materials and Methods

2.1. Substrates and raw materials

A 60CrMnMo steel plate, measuring 150 mm × 150 mm × 20 mm, was utilized as the substrate material. Powder-cored wires with varying niobium (Nb) contents (0.06 wt.%, 2 wt.%, 3 wt.%, 4 wt.%) and H08A steel strips were independently

selected as raw materials. The flux-cored wires were filled to approximately 33% capacity with uniformly mixed powder cores that had been sieved through a 60-mesh screen and subsequently blended for 12 hours using a V-type powder mixer to ensure homogeneity. Finally, the CXJ8-160 flux-cored wire molding machine was employed to produce flux-cored wire with a diameter of 3.2 mm from the powdered core and H08A steel strip mixture. The composition of the base material provided by the manufacturer is detailed in Table 1.

2.2. Preparation of surfacing alloys

Four types of surfacing alloys with varying niobium contents were fabricated on a 60CrMnMo steel plate using the submerged arc surfacing welding method. Prior to surfacing, the substrate surface was polished with coarse sandpaper and subsequently cleaned thoroughly with an ethanol solution. The flux-cored welding wire was then loaded into an automatic submerged arc welding machine for a three-layer surfacing process on the substrate's surface. This three-layer application effectively reduced the dilution of the surfacing alloy by the substrate. The parameters of the welding process are detailed in Table 2. A wire-cutting machine was employed to extract samples measuring 10 mm × 10 mm × 10 mm from the center of these four surfacing alloys, and the compositions of these flux-cored wire surfacing alloys were analyzed using a spark direct reading spectrometer, as presented in Table 3.

2.3. Characterization of microstructure and microhardness

Following the welding process, specimens measuring 10 mm × 10 mm × 10 mm were extracted from the central region of each set of surfacing alloys. The upper surface of the third layer of surfacing metal was precisely cut to achieve a flat surface, followed by employing the standard metallographic preparation procedure. Subsequently, polishing with sandpaper ranging from 80 to 2000 mesh was performed on the surfacing alloys' surface. Finally, a sample was subjected to polishing using a polishing machine and 0.1 μm diamond grinding paste, concluding with corrosion treatment utilizing a mixture consisting of hydrochloric

Table 1. Chemical composition of the substrate.

Element (wt.%)	C	Si	Mn	S	Cr	Ni	Mo	Fe
Substrate	0.55~0.65	0.2~0.6	0.5~1	≤0.03	0.8~1.2	0.2~1.5	0.2~0.6	Bal.

Table 2. Surfacing welding process parameters.

Current	Voltage	Wire Feed Speed	Travel Speed	Holding Time	Cooling Method
[A]	[V]	[mm/min]	[mm/min]	[sec]	
380	30	500	360	90	Air cooling

Table 3. Chemical composition of the submerged arc welding alloys.

Element (wt.%)	Cr	Nb	Mn	Mo	Ni	Si	C	Fe
1	8.22	0.06	2.19	1.31	0.29	0.75	0.62	Bal.
2	8.03	1.97	2.26	1.34	0.28	0.89	0.64	Bal.
3	8.32	3.05	2.29	1.34	0.34	0.89	0.62	Bal.
4	8.20	4.02	2.29	1.33	0.3	0.79	0.65	Bal.

acid and nitric acid in a ratio of 2:1. The microstructure of welded specimens was observed by an optical microscope. The crystal structure of welded specimens was determined by X-ray diffractometer with Cu-Kα as the ray source, 2θ ranging from 30 ° to 80 °, and scanning speed of 3 °/min. X-ray diffractometer and scanning electron microscope-energy dispersion spectrometer were used to characterize the structure and elemental composition of the sample, and the microhardness was determined by micro-Vickers hardness tester (20 points were taken at the same distance intervals along the weld direction at the heart, and their average values were taken).

2.4. Wear resistance measurements

The wear resistance of surfacing welding samples with varying Nb content was investigated using the Rtec friction and wear testing machine. The experimental parameters are presented in Table 4 (the hardness of the grinding balls is 700 HV). The coefficient of friction (COF) for each sample was recorded automatically by the computer. The 3D surface morphology and total volume loss of the samples were assessed using a 3D shape observation platform, while the volume wear rate was calculated according to the Archard equation[34].

$$k = \frac{V}{F_n d} \tag{1}$$

Where k is the wear rate in units of mm³/(N·m), V is the volume of the worn scar in units of mm³, F_n is the normal load in units of N, and d is the sliding distance in units of m.

3. Results and Discussion

3.1. Microstructure of the surfacing alloy

The XRD pattern in Figure 1 depicts surfacing alloys with varying Nb content. As shown in Figure 1, the surfacing alloy is primarily composed of Fe-Cr, γ-Fe, α'-Fe, and NbC. No diffraction peaks of Cr_7C_3 and $Cr_{23}C_6$ are observed in this figure, indicating that Cr_7C_3 and $Cr_{23}C_6$ are either rarely present or not present at all in the surfacing alloy. The black lines in Figure 1 indicate that the surfacing alloy containing 0.06 wt.% Nb is mainly composed of Fe-Cr, γ-Fe, and α'-Fe. The absence of a diffraction peak corresponding to NbC, suggests that NbC is either absent or present in an undetectable amount within the alloy. When the Nb content increases to 2 wt.%, both the NbC diffraction peak and the γ-Fe (111) diffraction peak appear, while the intensity of the γ-Fe (200) diffraction peak and the α'-Fe (110) diffraction peak decreases. As the Nb content increases from 2 wt.% to 4 wt.%, the intensity of the NbC and α'-Fe diffraction peaks gradually increases, while the intensity of the γ-Fe

diffraction peak gradually decreases. This indicates that the Nb content in the surfacing alloy is increasing, resulting in an increase in NbC and martensite, as well as a decrease in austenite. The maximum amount of NbC and martensite is achieved when the Nb content increases to 4 wt.%, while the austenite content decreases to its minimum level.

Figure 2 shows the distribution and morphology of NbC in surfacing alloys with different niobium additions. The presence of NbC was not observed in the 0.06 wt.% Nb surfacing alloy. As the Nb content increased from 2 wt.% to 4 wt.%, NbC precipitated in a short rod-like morphology at the grain boundary, and its quantity augmented with higher Nb content. The low solubility of Nb in the alloy leads to an increase in the nucleation rate and precipitation of NbC.

The scanning electron microscopy (SEM) images of surfacing alloys with varying Nb content were illustrated in Figure 3. Granular NbC, with limited presence, was found in the surfacing alloy containing 0.06 wt% Nb, accompanied by a relatively thick martensite and significant spacing between adjacent martensite strips, as depicted in Figure 3(a). As shown in Figure 3(b), with the gradual increase of Nb content from 0.06 wt.% to 2 wt.%, granular NbC transformed into short rod-like NbC, and the martensite became significantly refined and denser. As shown in Figure 3(d), when the Nb content of increases to 4 wt.%, the number of short-rod NbC particles increased, and their distribution became more uniform in the surfacing alloy.

Specimens with 0.06 wt.% Nb, 2 wt.% Nb, 3 wt.% Nb and 4 wt.% Nb were analyzed by EDS, as shown in Figure 4. The grayscale image areas in Figure 4(a)-(d) are martensite matrix, while the white phase was composed of Nb and C, specifically identified as NbC. As illustrated in Figure 4, chromium (Cr) predominantly exists in the matrix
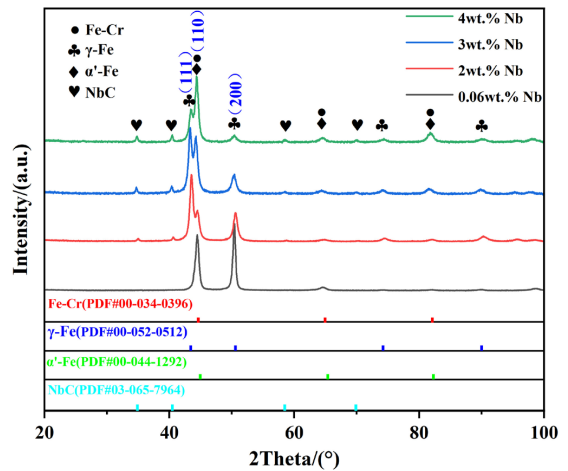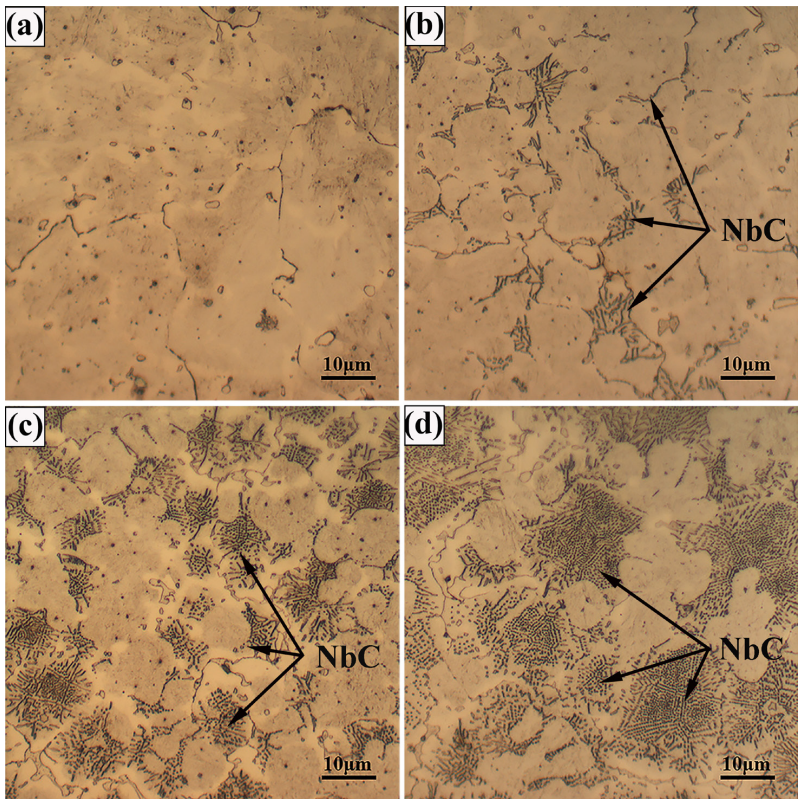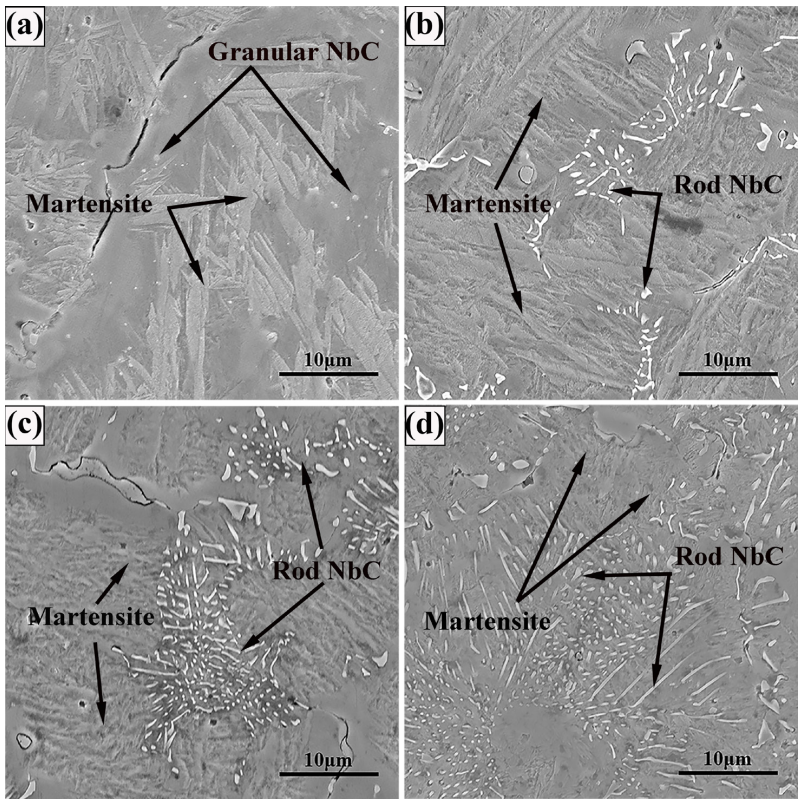

Figure 1. XRD patterns of the four surfacing alloys.

Table 4. Parameters used for submerged arc surfacing.

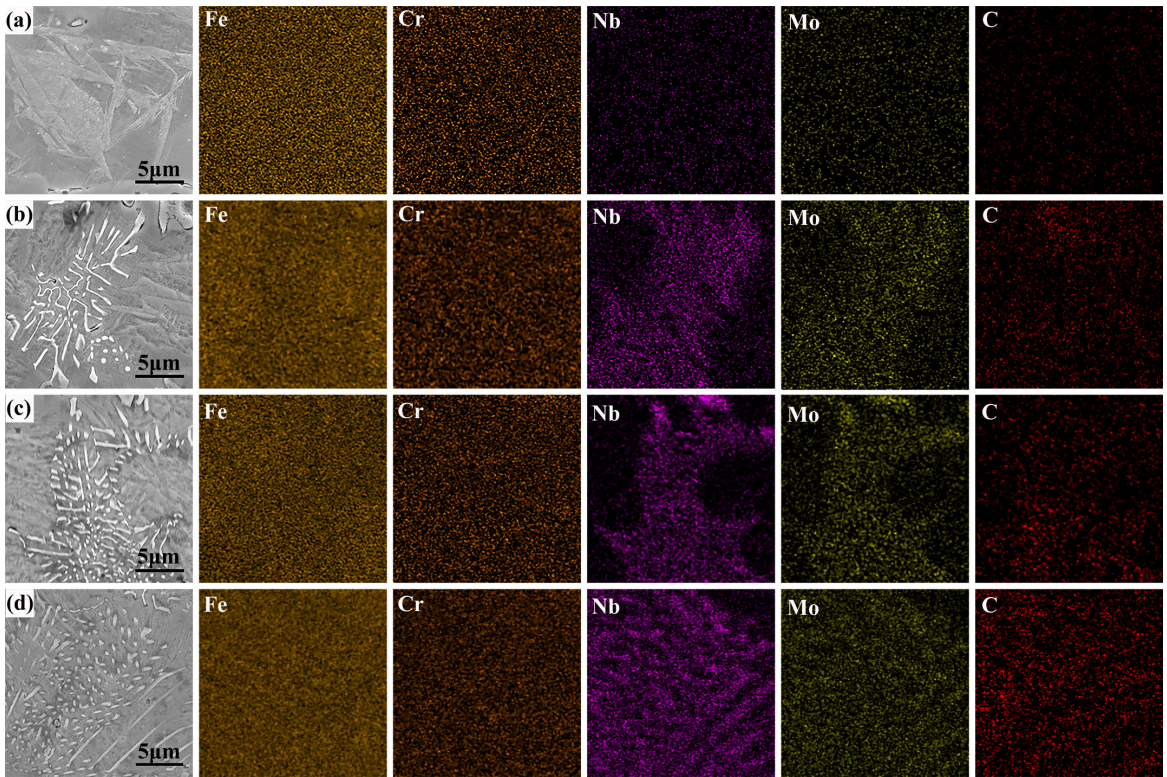| Parameters	Values	Parameters	Values
Test environment	Non-lubrication	Load	20 N
Grinding ball	GCR15	Sample size	15 mm×10 mm×10 mm
Friction speed	2 Hz	Test time	1800 sec

Figure 2. OM images of surfacing alloys: (a) 0.06 wt.% Nb, (b) 2 wt.% Nb, (c) 3 wt.% Nb, (d) 4 wt.% Nb.

Figure 3. SEM images of surfacing alloys: (a) 0.06 wt.% Nb, (b) 2 wt.% Nb, (c) 3 wt.% Nb, (d) 4 wt.% Nb.

Figure 4. EDS mapping of elements in surfacing alloys: (a) 0.06 wt.% Nb, (b) 2 wt.% Nb, (c) 3 wt.% Nb, (d) 4 wt.% Nb.

as a solid solution. This phenomenon can be attributed to the strong affinity of both niobium (Nb) and Cr for carbon (C), which facilitates the formation of stable compounds. However, Nb exhibits superior carbide-forming capability, preferentially bonding with C to form compounds such as NbC. Consequently, this process consumes a significant amount of C within the matrix, reducing the availability of C for Cr to combine with, thereby inhibiting the precipitation of Cr carbides. As a result, the proportion of Cr present as a solid solution in the alloy matrix is increased, enhancing its solid solubility. The preferential consumption of C by NbC significantly diminishes the available C for Cr, not only decreasing the likelihood of Cr forming carbides but also promoting a more uniform distribution of C within the matrix, thus mitigating C segregation. Moreover, the precipitation of NbC indirectly influences the distribution of Cr.

Experimental results demonstrate that Cr and C exhibit mutual repulsion within the α-Fe matrix, with their interaction decreasing as the distance between them increases. Upon NbC precipitation, a significant amount of C is consumed, further diminishing the interaction between Cr and C, resulting in a more homogeneous distribution of Cr within the matrix. During the NbC precipitation process, Cr may be "extruded" or redistributed away from the interface between NbC and the matrix, thereby reducing its segregation at this interface. This redistribution enhances interfacial bonding and optimizes the microstructure of the alloy. Ultimately, the presence of Cr in the matrix as a solid solution achieves solid solution strengthening through lattice distortion and dislocation hindrance, thereby improving the strength and hardness of the alloy.

Therefore, the incorporation of Nb and the subsequent precipitation of NbC substantially influence the interaction between Cr and C by altering the distribution of carbon, inhibiting the formation of chromium carbides, and optimizing the distribution of chromium. This ultimately enhances the overall properties of the alloy.

Additionally, a significant quantity of molybdenum (Mo) was observed to be fully dissolved within NbC. The solid solution of Mo in NbC can augment the volume fraction of NbC precipitation, refine the size of NbC particles, and enhance the strengthening effect through precipitation. As shown in Figure 4(a), no rod-like NbC precipitates were found in the 0.06 wt.% Nb surfacing alloy, and Nb elements were less and dispersed in the matrix together with other alloying elements. However, a significant number of NbC precipitates were observed in the surfacing alloys containing 2 wt.% Nb, 3 wt.% Nb and 4 wt.% Nb. As the Nb content increases, both the quantity and size of NbC particles show a continuous refinement. Notably, the surfacing alloy with 4 wt.% Nb exhibits the highest amount of NbC precipitates, filling the entire area.

The TEM images and SAED images of martensite and NbC in 0.06 wt.% Nb and 4 wt.% Nb surfacing alloys are presented in Figure 5. The martensite of the 0.06 wt.% Nb surfacing alloy, as depicted in Figure 5(a), exhibits a significant size with a width of up to 400 nm. Moreover, an abundance of dislocation plugging can be observed within the martensite, indicating its dislocation martensite nature. Dislocation martensite is commonly found in low carbon steel due to the increased presence of alloying elements that facilitate the transformation of carbon from solid solution into
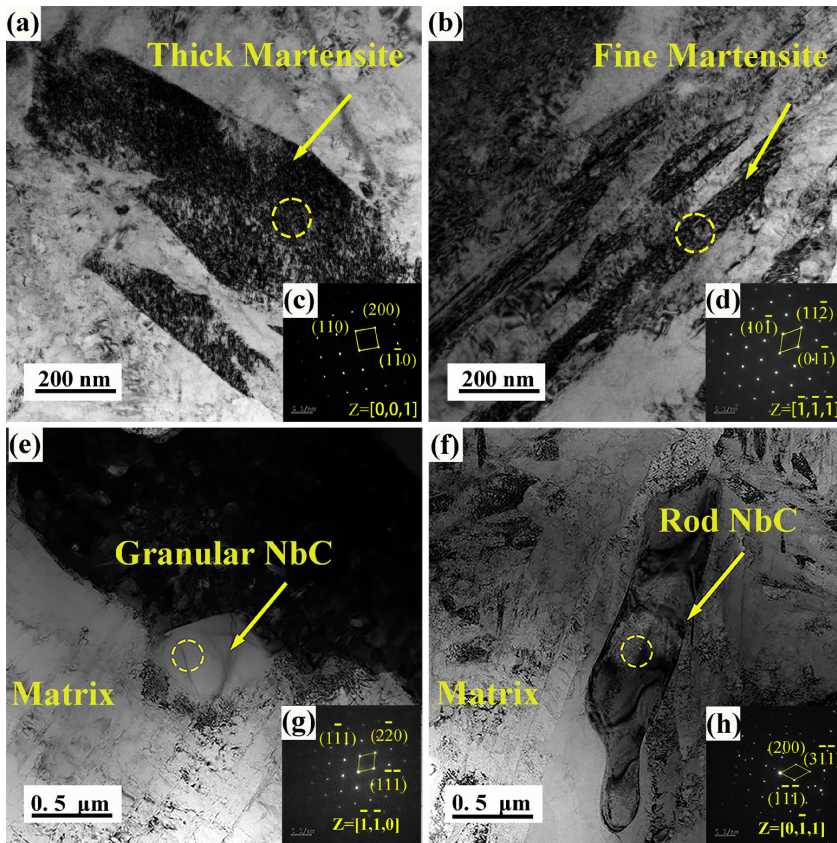
Figure 5. TEM images of martensite of the surfacing alloys of (a) 0.06 wt.% Nb, (b) 4 wt.% Nb and SAED patterns of (c) 0.06 wt.% Nb and (d) 4 wt.% Nb; TEM images of NbC of the surfacing alloy of (e) 0.06 wt.% Nb, (f) 4 wt.% Nb and SAED patterns of (g) 0.06 wt.% Nb and (h) 4 wt.% Nb.

carbides. This process effectively reduces the carbon content in austenite, thereby favoring the formation of dislocation martensite. The martensite of the 4 wt.% Nb surfacing alloy, as depicted in Figure 5(b), exhibits significant refinement, with a width measuring approximately 100nm. Figure 5(e) and Figure 5(f) depict the morphological characteristics of NbC in 0.06 wt%Nb and 4 wt.% Nb surfacing alloys, respectively. The granular precipitation of NbC in 0.06 wt%Nb surfacing alloys can be attributed to the relatively low concentration of Nb, while the rod-shaped precipitation observed in 4 wt.% Nb surfacing alloys is a result of the higher content of Nb. It should be noted that both the granular NbC phase and rod-shaped NbC possess face-centered cubic structures, with their respective crystallographic orientations being $[\bar{1}\bar{1}0]$ and $[0\bar{1}1]$.

The TEM results of surfacing alloy with 4 wt.% Nb are shown in Figure 6. About 200 nm-wide NbC reinforcing phase was produced in situ, and no other phase were generated at the interface between the NbC and the matrix in Figure 6(a) and (c). According to the EDS results presented in Figure 6(b), it can be observed that this phase is predominantly composed of Nb and C. HR-TEM and SAED diagrams of the NbC phase are shown in Figure 6(c) and (d), respectively. The resemblance between the diffraction pattern with that of the NbC from the $[\bar{1}\bar{1}0]$ direction provides further evidence that this phase was NbC (FCC, a=b=c=0.44 nm).

Analyzing Figure 2 - Figure 4 reveals a notable increase in the quantity of NbC carbides with rising Nb content. This phenomenon can be attributed to an enhanced nucleation rate of carbides as Nb content increases, leading to a corresponding rise in the volume fraction of NbC[35]. Given that the solubility of Nb in austenite is quite low[15,36], niobium predominantly exists within the alloy as MC carbides. Following submerged arc welding and during subsequent continuous cooling processes, NbC initially precipitates from the liquid phase before austenite grains commence their growth. The distribution of NbC along austenite grain boundaries serves to pin these boundaries, thereby inhibiting further growth of austenite grains[37,38]. A higher concentration of niobium carbide results in more pronounced pinning effects on the grain boundaries, which contributes to finer austenite . The dimensions of martensite bands are closely linked to those of the primary austenite grains; thus, reduced grain size leads to an increased number of grain boundaries. This increment diminishes the driving energy necessary for transforming austenite into martensite while simultaneously elevating martensite nucleation frequency— thereby facilitating martensite transformation and yielding finer and denser martensite structures. Additionally, new precipitates of NbC emerge at the grain boundaries within the austenitic matrix; these act as non-spontaneous nucleation sites for martensite formation by destabilizing supercooled austenite and promoting its transition into martensite phases[39].
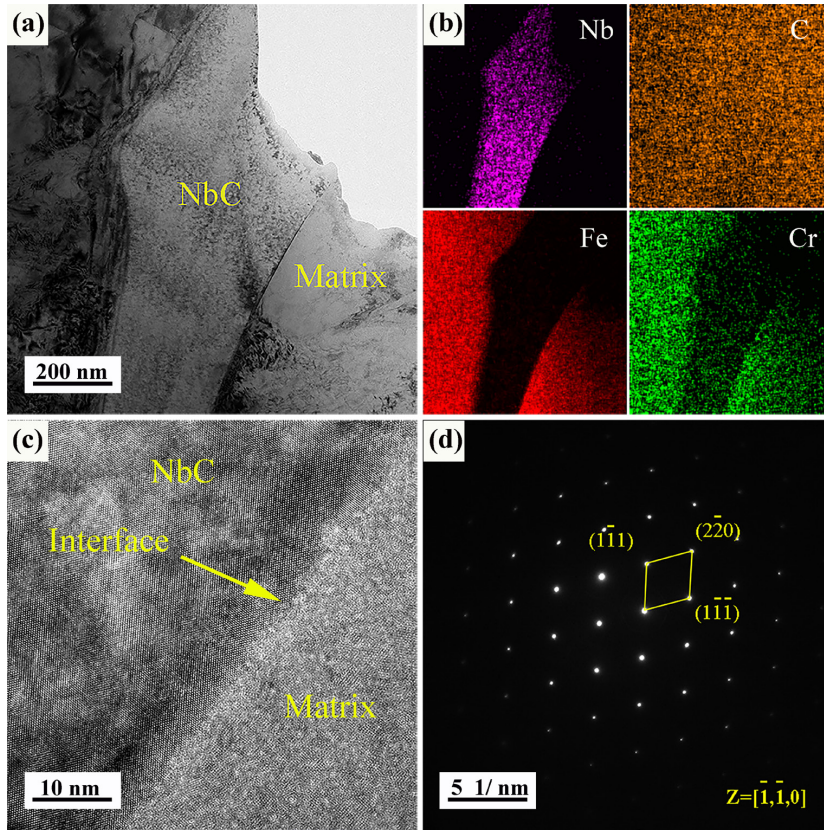
Figure 6. TEM images of the 4 wt.% Nb surfacing alloy: (a) bright field image, (b) EDS. maps of Nb, C, Fe, and Cr; (c) HR-TEM image of the NbC phase and (d) SAED pattern of NbC.

As illustrated in Figure 7, it becomes evident that surface alloy hardness is significantly enhanced through synergistic contributions from both increased precipitation of NbC and refinement within the martensite structure.

3.2. Hardness and wear resistance of surfacing alloy

The XRD results demonstrate that the variation in Nb content significantly impacts the matrix of the surfacing alloy. As the Nb content increases, there is a gradual transformation from austenite to martensite. The average Vickers hardness of surfacing alloys with varying Nb content is illustrated in Figure 7. As the Nb content increases, there is an enhanced transformation from austenite to martensite, resulting in a continuous increase in the hardness of the surfacing alloy. The highest hardness value (627 HV) is observed for the 4 wt.% Nb surfacing alloy, followed by a slightly lower value (598 HV) for the 3 wt.% Nb surfacing alloy. The lowest hardness value (221 HV) is exhibited by the 60CrMnMo substrate, less than half of the hardness of 0.06 wt.% Nb surfacing alloy(488 HV). Little research has been conducted on Fe-Cr-C surfacing alloys with carbon content of 0.6 wt.%. Filipovic et al.[22] increased the hardness of Fe-Cr-C cast iron to 570 HV by adding 3.17 wt.% Nb, which is 28 HV lower than the hardness of the 3 wt.% Nb surfacing alloy studied in this research. Meanwhile, its carbon and chromium contents are much higher than those of the surfacing alloys studied in this research. In addition, Xiao Jin-Kun et al.[40] found
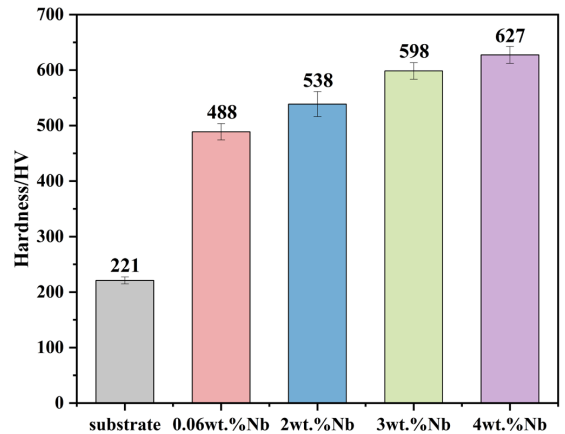
Figure 7. Average hardness of the four surfacing alloys.

that the hardness of the CoCrFeMnNiCx high-entropy alloy with a carbon content of 0.6 wt.% is 550 HV. However, the hardness of the surfacing alloy studied in this research can reach 627 HV, thus the surfacing alloy studied in this research has certain advantages compared with similar products.

The friction coefficient (COF) curve of the substrate and surfacing alloys at room temperature is presented in Figure 8. In the initial stage of wear, there is a rapid increase in friction coefficient due to significant changes in surface roughness of the surfacing alloy until it reaches its peak.
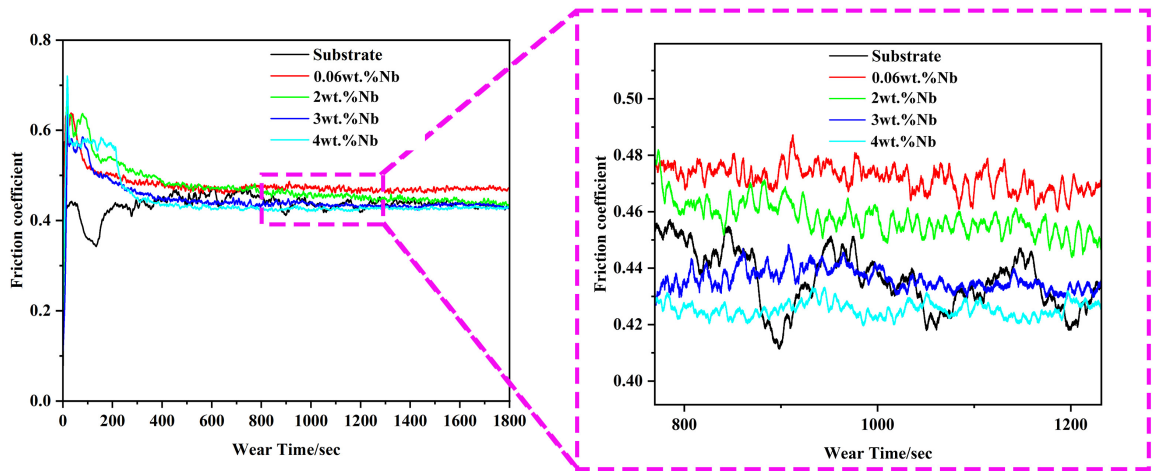
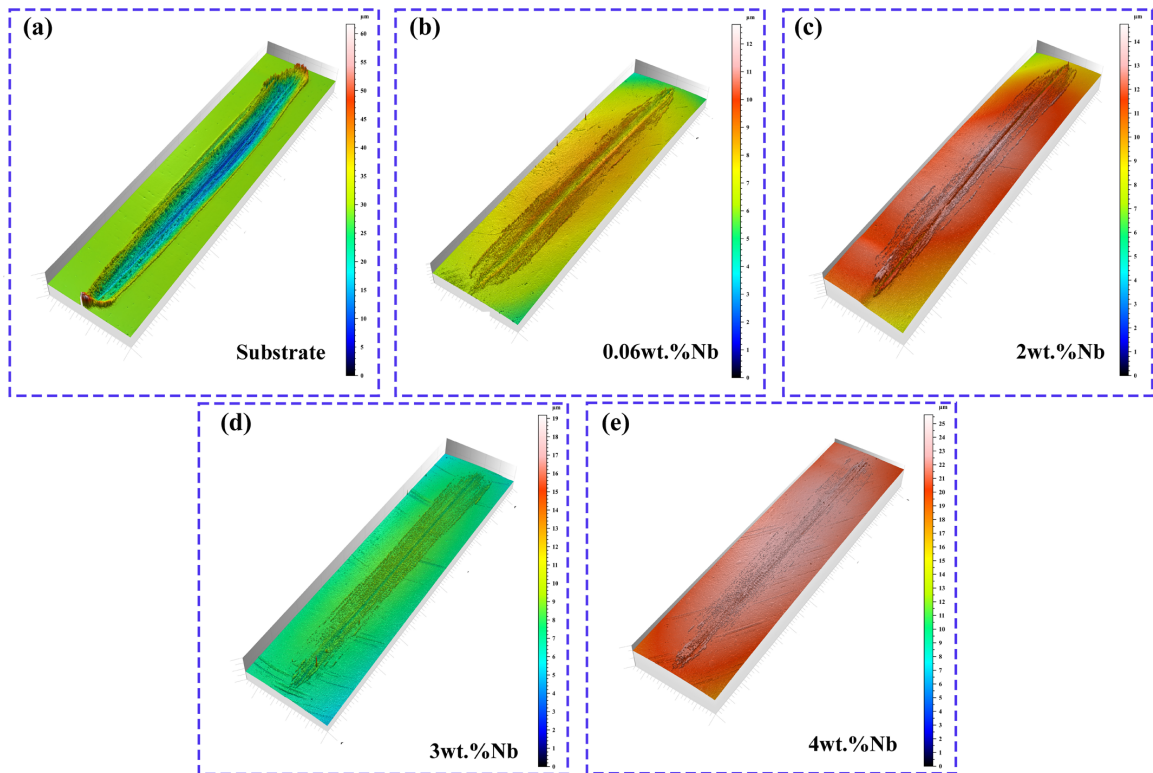**Figure 8.** Friction coefficient (COF) curve of 60CrMnMo substrate and the four surfacing alloys.

Figure 9. 3D morphology of the wear surface of 60CrMnMo substrate and the four surfacing alloys.

As testing time increases, the friction coefficient gradually decreases and eventually stabilizes after approximately 400 seconds. However, the COF curve of the substrate exhibits a significant decrease after reaching its peak and subsequently increases to another peak. Moreover, the COF fluctuates continuously during the subsequent wear process, indicating poor stability. This phenomenon can be attributed to the fact that during the initial stages of wear, wear debris generated by friction becomes embedded in the grooves created by grinding balls, thereby reducing surface roughness and consequently lowering the COF. As the

friction and grinding time increases, more and more abrasive debris is produced, and a large amount of debris is trapped in the contact area by the grooves, leading to an increase in the number of particles between the contact surfaces, thus causing the COF to start increasing. It is worth noting that the surfacing alloy with 4 wt.% Nb reaches the steady state first, exhibiting the lowest COF of 0.42. The surfacing alloy with 3 wt.%Nb shows a slightly higher COF of 0.45. On the other hand, the surfacing alloy containing 0.06 wt.% Nb exhibits the highest COF of 0.47. Furthermore, it should be noted that the surfacing alloy with 2 wt.%Nb does not reach

a steady state within the initial wear period of up to 1800 seconds and demonstrates a decreasing trend in COF. When assessing the adhesive wear performance of the coating, the evaluation criterion is established as the COF rather than weight loss. A lower COF indicates superior resistance to adhesive wear. Consequently, the 4 wt.% Nb surfacing alloy exhibits optimal adhesive wear resistance.

Figure 9 illustrates the 3D morphology of the wear surface of 60CrMnMo substrate and surfacing alloys with varying Nb content. The substrate exhibits the most severe wear, with noticeable accumulation of debris at both ends. In contrast, the surfacing alloys with varying Nb content show minimal signs of wear. The wear rate and average wear depth of both the substrate and surfacing alloy are depicted in Figure 10. The substrate exhibits the highest wear rate (736.3×10^{-5} mm^{3}N^{-1}m^{-1}) and average wear depth (8.67 μm), significantly surpassing those of the four types of surfacing alloys. As the Nb content increases from 0.06 wt.% to 4 wt.%, both the wear rate and average wear depth of the surfacing alloy consistently decrease. Among the four types of surfacing alloys, the 4 wt.% Nb surfacing alloy demonstrates the lowest wear rate (6.05×10^{-5} mm^{3}N^{-1}m^{-1}), while the 0.06 wt.% Nb surfacing alloy exhibits the highest wear rate (12.56×10^{-5} mm^{3}N^{-1}m^{-1}). The wear rate of the 4 wt.% Nb surfacing alloy is half that of its counterpart with a Nb content of 0.06 wt.% This indicates that the wear resistance

of a 4wt.%Nb surfacing alloy is twice as high as that of a 0.06 wt.% Nb surfacing alloy.

Figure 11 shows the SEM images of the wear track of the surfacing alloy after wear. The wear width of the 0.06 wt.% Nb surfacing alloy exhibits the highest value (1076.9336 μm), while the wear width of the 4 wt.% Nb surfacing alloy demonstrates the lowest value (911.7808 μm). Furthermore, there is a gradual decrease in wear width as the Nb content increases. The middle of the four types of
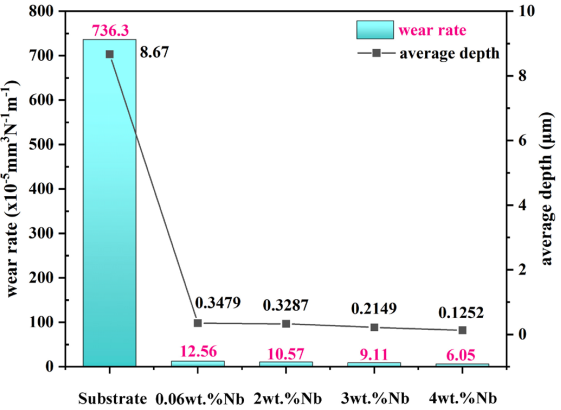

Figure 10. Wear rate and average wear depth of the substrate and the four surfacing alloys.
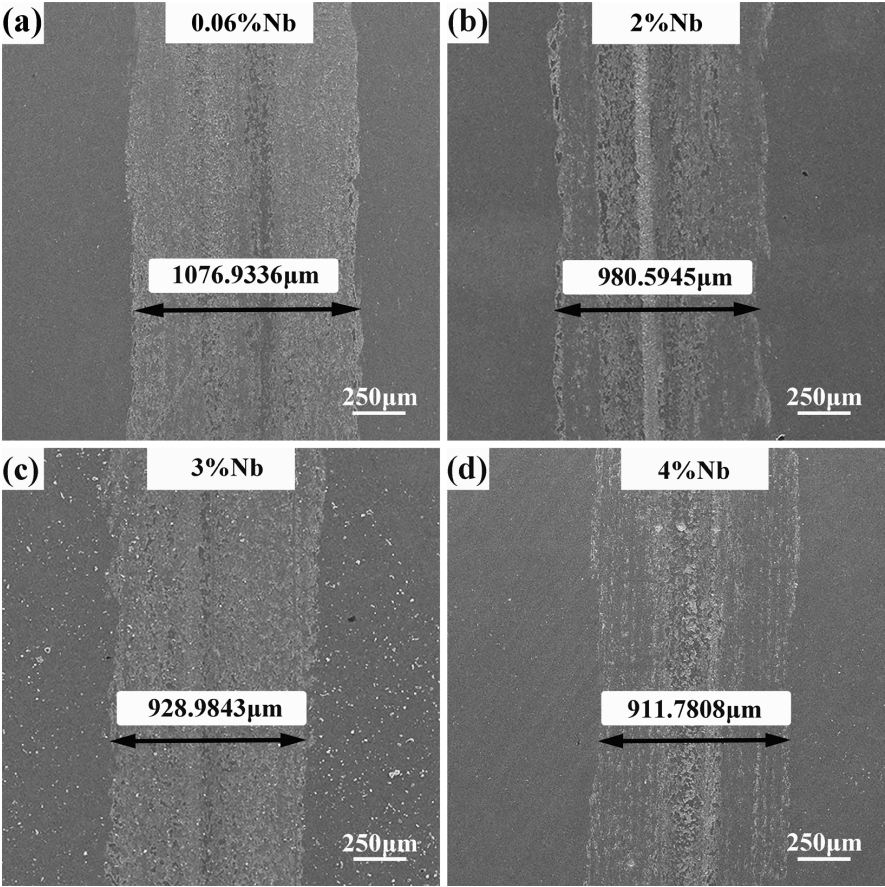

Figure 11. SEM images of the four worn surfacing alloys.

surfacing alloys exhibits a pronounced wear mark, attributed to the grinding ball's largest diameter circle and its interaction with the surfacing alloy. It is noteworthy that the 4 wt.% Nb surfacing alloy predominantly displays shallow wear marks across most areas, indicating superior wear resistance compared to other surfacing alloys.

Figure 12 shows the SEM images of wear surfaces of surfacing alloys with different Nb content after friction and wear tests. The upper left image in Figure 12(a)-(d) represents the secondary electron images obtained by magnifying the selected area within the yellow box, while the upper right image represents the back scattered electron image obtained by magnifying the same selected area within the yellow box. The four types of surfacing alloys with varying niobium content exhibit fracture plastic deformation along the reciprocating direction of the grinding ball, which is a characteristic manifestation of adhesive wear. The wear debris of varying shapes and sizes were also observed on the surfacing alloy's worn surface. The oxygen element in position A is observed to be higher, as depicted in Figure 12(b), which, based on the EDS analysis (Figure 13(b)), suggests that the debris present on the surface is predominantly oxide. The layered nature of the oxide found on the wear surface indicates that oxidative wear has occurred. Additionally, no conspicuous white NbC precipitates were observed in the

back-scattered electron image of the wear surface of the 0.06 wt.% Nb surfacing alloy, whereas varying amounts of NbC precipitates were detected in the 2 wt.% Nb, 3 wt.% Nb, and 4 wt.% Nb surfacing alloys. Furthermore, among these alloys, the 4 wt.% Nb surfacing alloy exhibited a higher quantity and more uniform dispersion of NbC precipitated phase (indicated by yellow circle in Figure 12). The numerous and finer precipitated NbC phases exhibit a larger contact area with the grinding ball, resulting in higher hardness and wear resistance compared to the substrate. Consequently, increasing the number of NbC effectively reduces the wear of the matrix of the 4 wt.% Nb surfacing alloy.

To investigate the wear mechanism and the influence of the NbC phase on the wear behavior of surfacing alloys at room temperature, we conducted an analysis of the wear surfaces of four distinct surfacing alloys with varying compositions using Energy Dispersive Spectroscopy (EDS). At a Nb content of 0.06 wt.%, The formation of the NbC phase in the surfacing alloy is minimal, leading to an absence of hard phases in the matrix that could mitigate wear, which consequently resulted in significant degradation of the surfacing alloy. There is a large gray area in Figure 13(a), with a relatively uniform brightness, indicating that the surface of the 0.06 wt.% Nb surfacing alloy is relatively flat after wear. With the increase of Nb
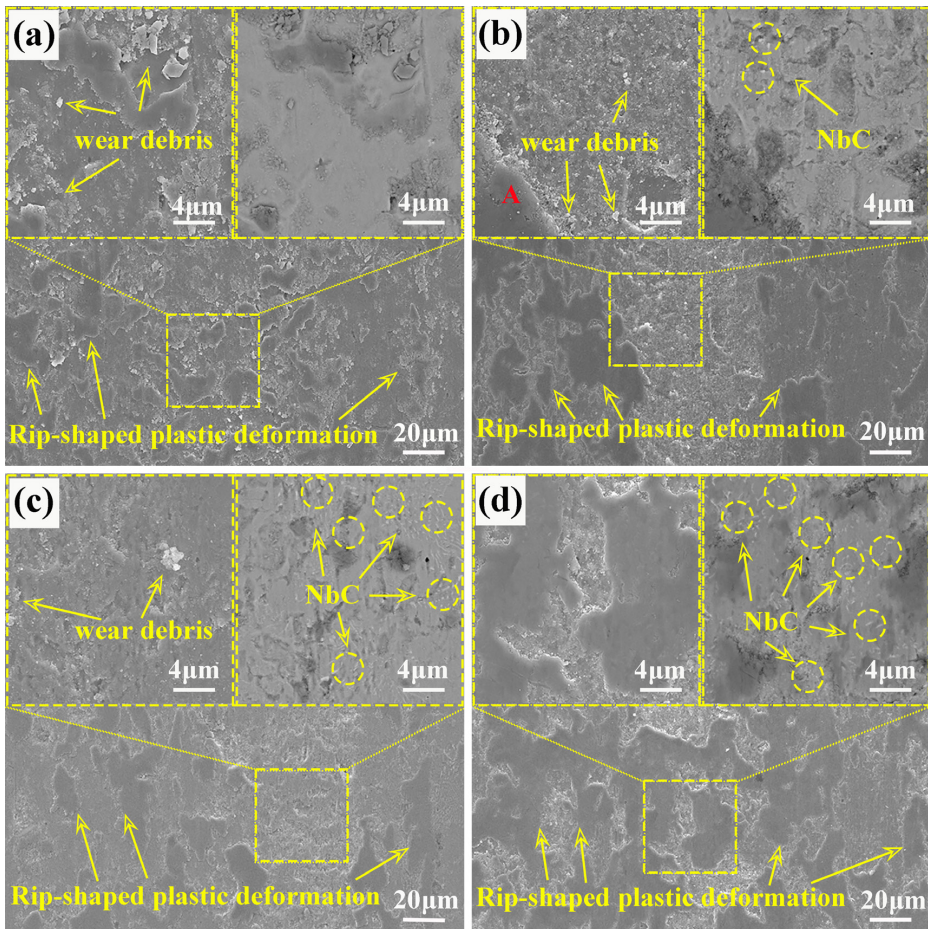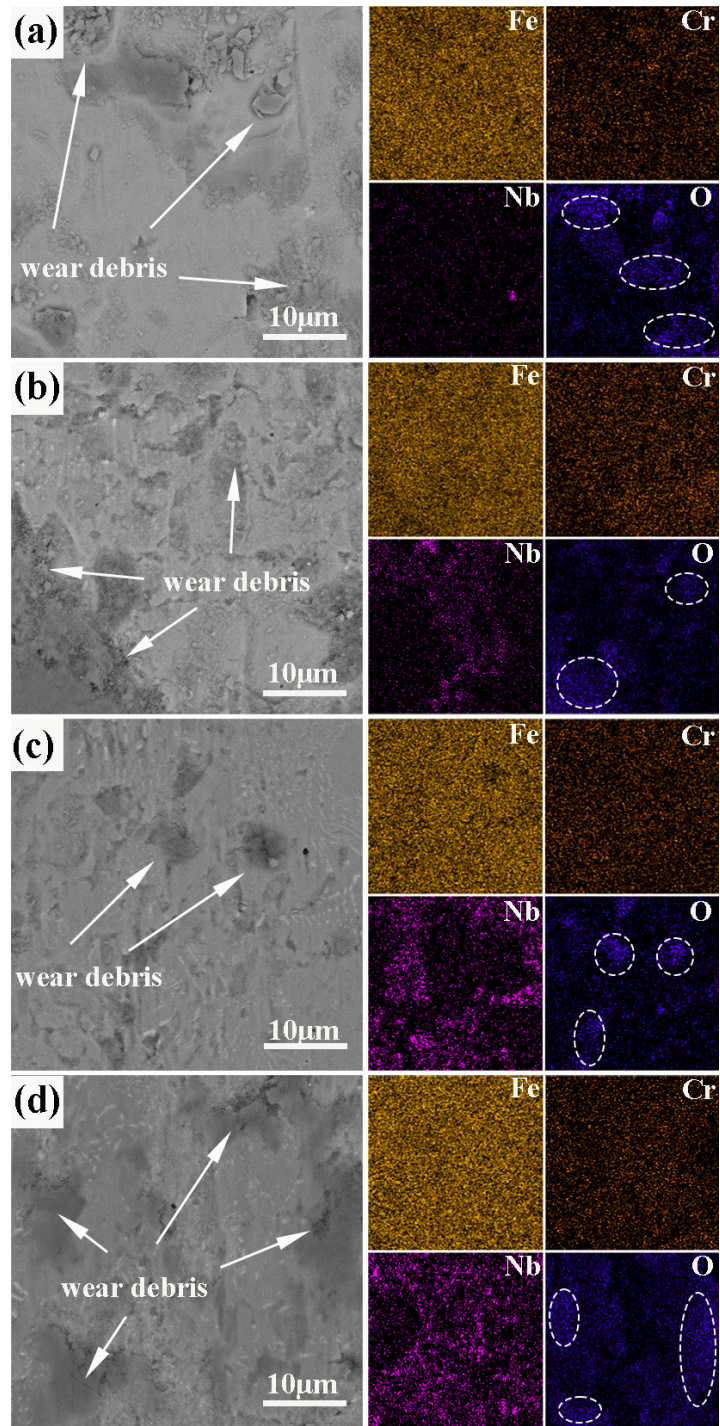

**Figure 12.** SE and BSE images of the four worn surfacing alloys.

Figure 13. BSE images and corresponding EDS mappings of the worn surfacing alloys: (a) 0.06 wt.% Nb, (b) 2 wt.% Nb, (c) 3 wt.% Nb, (d) 4 wt.% Nb.

content, the precipitation of NbC increases, which provides stronger support to the matrix and stronger resistance to wear, thus reducing the wear of the alloy. In Figure 13(b)-(d), a large number of bright particles can be observed, which are protruding NbC particles that hinder wear and protect the matrix. Many black areas can also be observed in the figure, which are caused by the accumulation of wear debris

and oxidation. It is worth noting that no NbC particles or plow grooves were found in Figure 13(a), and the number of NbC particles increased in Figure 13(b)-(d), but no plow grooves were found, indicating that abrasive wear did not occur in the wear process of the four surfacing alloys. In addition, according to EDS analysis, the area where the white ellipse is located in the figure is enriched with oxygen
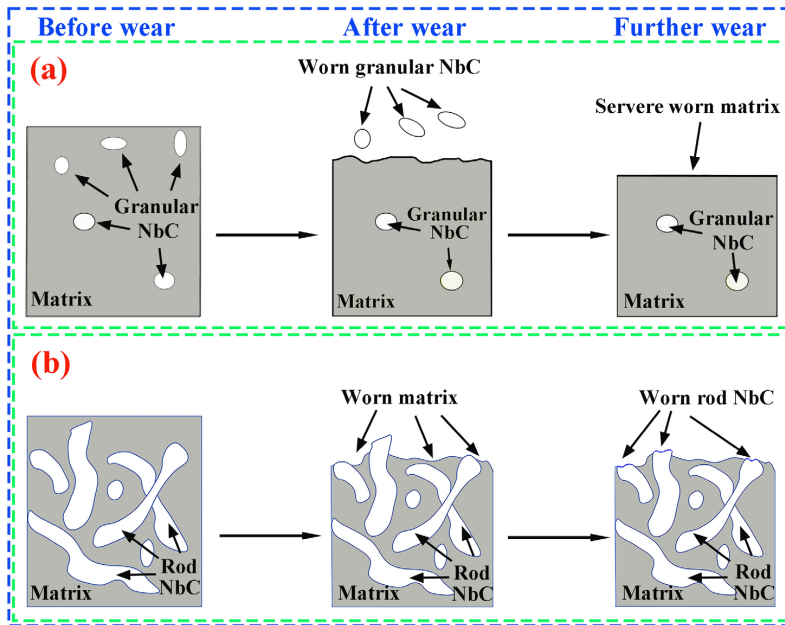
Figure 14. Wear mechanism diagrams of the surfacing alloys: (a) 0.06 wt.% Nb, (b) 4 wt.% Nb.

elements, which are oxidation products generated during the friction and wear process, mainly composed of Fe and O. This indicates that oxidation wear occurred in the friction and wear process of the surfacing alloys.

In the case of the 0.06 wt.% Nb surfacing alloy, its low hardness, limited number of NbC precipitates, and small particle-like morphology render it ineffective in protecting the softer base material from wear, resulting in significant plastic deformation and a high wear rate under load[41]. Conversely, the 4 wt.% Nb surfacing alloy exhibits higher hardness and a greater abundance of NbC precipitates in the form of short rods. This characteristic renders the 4 wt.% Nb surfacing alloy less susceptible to wear compared to its 0.06 wt.% counterpart during operational conditions. The wear behavior of both alloys is illustrated in Figure 14. In the case of the 0.06 wt.% Nb surfacing alloy, only a limited quantity of particle-like NbC precipitates are present; their morphology does not significantly enhance strengthening effects on the base material, which also provides inadequate support. Consequently, during wear processes, these particles tend to be worn away along with the base material, failing to effectively mitigate wear. Conversely, In the 4 wt.%Nb surfacing alloy, there are more NbC particles and they are smaller in size, which results in a larger contact area between NbC particles and grinding balls during wear. This allows the surfacing alloy to withstand higher loads and protect the base material more effectively, reducing its wear. Additionally, the NbC particles in the 4 wt.% Nb surfacing alloy are embedded in the base material in the form of short rod-like structures, which allow the softer base material to be closely bonded to the harder NbC particles. During wear, the softer base material is worn away first, while the harder NbC particles gradually protrude from the surface and bear part of the load, reducing the contact area between the base material and the grinding balls and effectively preventing plastic deformation and additional wear. At the same time,

since the NbC particles are embedded in the base material in the form of rod-like structures at a depth, the softer base material provides good support for the harder rod-like NbC particles, making the short rod-like NbC particles have stronger anti-abrasion ability. Therefore, during wear, these short rod-like NbC particles mainly experience minor wear rather than falling off, without forming new abrasive particles, thus avoiding further damage to the surfacing alloy. This also explains why no plow grooves were observed in Figure 13.

4. Conclusion

Four types of surfacing alloys with varying Nb content were prepared through submerged arc surfacing using self-cored welding wire. The microstructure, microhardness, and wear resistance among them were analyzed, leading to the following conclusions:

1. The morphology, quantity, size, and distribution position of NbC in surfacing alloys vary with different Nb contents. At a low Nb content of only 0.06 wt.%, the amount of granular NbC is minimal. As the Nb content increases to 2 wt.%, short rod-shaped NbC precipitates with an increased amount. When the Nb content reaches 4 wt.%, the precipitation is maximized and more dispersed in its distribution.

2. With the increase in Nb content, the hardness of the surfacing alloy continues to rise. The average micro-Vickers hardness of 4 wt.%Nb surfacing alloy is 627 HV, which is 139 HV higher than that of 0.06 wt.% Nb surfacing alloy.

3. The wear rate, wear depth, and wear width of surfacing alloys decrease with an increase in Nb content, leading to an enhancement in wear resistance. Specifically, the wear resistance of a 4 wt.% Nb surfacing alloy is twice as high as that

of a 0.06 wt.% Nb surfacing alloy and 120 times higher than that of the 60CrMnMo substrate.

4. (4) The predominant wear mechanisms of the Fe-8.2wt.%Cr-0.6wt.%C-Xwt.%Nb surfacing alloy at room temperature are primarily adhesive wear and oxidative wear.

5. Acknowledgments

Data Availability

No data was used for the research described in the article.

References

1. Chen CX, Zuo YQ, Liu BX, Xue HT, Ma B, Li XC. Microstructure and wear resistance of nano titanium dioxide strengthening hardfacing material. Vacuum. 2019;162:175-82. http://doi.org/10.1016/j.vacuum.2019.01.045.

2. Zhu S, Yuan W, Cong J, Guo Q, Chi B, Yu J. Analysis of regional wear failure of crankshaft pair of heavy duty engine. Eng Fail Anal. 2023;154:107635. http://doi.org/10.1016/j.engfailanal.2023.107635.

3. Findik F. Latest progress on tribological properties of industrial materials. Mater Des. 2014;57:218-44. http://doi.org/10.1016/j.matdes.2013.12.028.

4. Wang D, Sun J, He Q, Si J, Shi T, Li F, et al. Failure analysis and improvement measures for crankshaft connecting rod of refrigerator compressor. Eng Fail Anal. 2022;141:106585. http://doi.org/10.1016/j.engfailanal.2022.106585.

5. Singh A, Singh R. A review of effect of welding parameters on the mechanical properties of weld in submerged arc welding process. Mater Today Proc. 2020;26:1714-7. http://doi.org/10.1016/j.matpr.2020.02.361.

6. Zahiri R, Sundaramoorthy R, Lysz P, Subramanian C. Hardfacing using ferro-alloy powder mixtures by submerged arc welding. Surf Coat Tech. 2014;260:220-9. http://doi.org/10.1016/j.surfcoat.2014.08.076.

7. Buchely M, Gutierrez J, Leon L, Toro A. The effect of microstructure on abrasive wear of hardfacing alloys. Wear. 2005;259(1-6):52-61.

8. Orečný M, Buršák M, Viňáš J. The influence of heat treatmemnt on the abrasive wear resistnace of a construction and a tool steel. Metalurgija. 2015;54(1):191-3.

9. Wiengmoon A. Carbides in high chromium cast irons. Naresuan University Engineering Journal. 2011;6(1):64-71.

10. Chen JH, Hsieh CC, Hua PS, Chang CM, Lin CM, Wu PTY, et al. Microstructure and abrasive wear properties of Fe-Cr-C hardfacing alloy cladding manufactured by Gas Tungsten Arc Welding (GTAW). Met Mater Int. 2013;19(1):93-8. http://doi.org/10.1007/s12540-013-1015-4.

11. Liu S, Zhou Y, Xing X, Wang J, Ren X, Yang Q. Growth characteristics of primary M_7C_3 carbide in hypereutectic Fe-Cr-C alloy. Sci Rep. 2016;6(1):32941. http://doi.org/10.1038/srep32941. PMid:27596718.

12. Fan C, Chen MC, Chang CM, Wu W. Microstructure change caused by (Cr, Fe) 23C6 carbides in high chromium Fe-Cr-C

13. Yüksel N, Şahin S. Wear behavior–hardness–microstructure relation of Fe–Cr–C and Fe–Cr–C–B based hardfacing alloys. Mater Des. 2014;58:491-8. http://doi.org/10.1016/j.matdes.2014.02.032.

14. Zhou Y, Yang Y, Li D, Yang J, Jiang Y, Ren X, et al. Effect of titanium content on microstructure and wear resistance of Fe-Cr-C hardfacing layers. Weld J. 2012;91(8):229-35.

15. Baik H, Loper C Jr. The influence of niobium on the solidification structure of Fe-C-Cr alloys. Trans Am Foundrymen's Soc. 1988;96:405-12.

16. Fiset M, Peev K, Radulovic M. The influence of niobium on fracture toughness and abrasion resistance in high-chromium white cast irons. J Mater Sci Lett. 1993;12(9):615-7. http://doi.org/10.1007/BF00465569.

17. He Xing C, Zhe Chuan C, Jin Cai L, Huai Tao L. Effect of niobium on wear resistance of 15% Cr white cast iron. Wear. 1993;166(2):197-201. http://doi.org/10.1016/0043-1648(93)90262-K.

18. Kesri R, Durand-Charre M. Phase equilibria, solidification and solid-state transformations of white cast irons containing niobium. J Mater Sci. 1987;22(8):2959-64. http://doi.org/10.1007/BF01086497.

19. Loper C, Baik H. Influence of molybdenum and titanium on the microstructures of Fe-C-Cr-Nb white cast irons. In: 93 rd AFS Casting Congress; 1989; San Antonio, TX. Proceedings. Schaumburg: American Foundry Society; 1989.

20. Zhi X, Xing J, Fu H, Xiao B. Effect of niobium on the as-cast microstructure of hypereutectic high chromium cast iron. Mater Lett. 2008;62(6-7):857-60. http://doi.org/10.1016/j.matlet.2007.06.084.

21. Correa EO, Alcântara NG, Valeriano LC, Barbedo ND, Chaves RR. The effect of microstructure on abrasive wear of a Fe-Cr-C-Nb hardfacing alloy deposited by the open arc welding process. Surf Coat Tech. 2015;276:479-84.

22. Filipovic M, Kamberovic Z, Korac M, Gavrilovski M. Microstructure and mechanical properties of Fe-Cr-C-Nb white cast irons. Mater Des. 2013;47:41-8.

23. Paz-Triviño F, Buitrago-Sierra R, Santa-Marín JF. Wear resistance and hardness of nanostructured hardfacing coatings. Dyna (Medellin). 2020;87(214):146-54.

24. Chang CM, Chen YC, Wu W. Microstructural and abrasive characteristics of high carbon Fe–Cr–C hardfacing alloy. Tribol Int. 2010;43(5-6):929-34.

25. Tippayasam C, Taengwa C, Palomas J, Siripongsakul T, Thaweechai T, Kaewvilai A. Effects of flux-cored arc welding technology on microstructure and wear resistance of Fe-Cr-C hardfacing alloy. Mater Today Commun. 2023;35:105569.

26. Correa E, Alcântara N, Valeriano L, Barbedo N, Chaves R. The effect of microstructure on abrasive wear of a Fe-Cr-C-Nb hardfacing alloy deposited by the open arc welding process. Surf Coat Tech. 2015;276:479-84.

27. Chung R, Tang X, Li D, Hinckley B, Dolman K. Microstructure refinement of hypereutectic high Cr cast irons using hard carbide-forming elements for improved wear resistance. Wear. 2013;301(1-2):695-706.

28. Menon R. New developments in hardfacing alloys. Weld J. 1996;75:43-9.

29. Yang J, Tian J, Hao F, Dan T, Ren X, Yang Y, et al. Microstructure and wear resistance of the hypereutectic Fe-Cr-C alloy hardfacing metals with different La_2O_3 additives. Appl Surf Sci. 2014;289:437-44.

30. Liu S, Shi Z, Xing X, Ren X, Zhou Y, Yang Q. Effect of Nb additive on wear resistance and tensile properties of the hypereutectic Fe-Cr-C hardfacing alloy. Mater Today Commun. 2020;24:101232.

31. Su S, Song R, Quan S, Li J, Wang Y, Cai C, et al. A Fe-Cr-C steel based on gradient scale precipitation hardening: hardening and toughening mechanism of multistage heat treatment. J Alloys Compd. 2023;946:169355. http://doi.org/10.1016/j.jallcom.2023.169355.

32. Zhao C, Zhou Y, Xing X, Liu S, Ren X, Yang Q. Investigation on the relationship between NbC and wear-resistance of Fe matrix composite coatings with different C contents. Appl Surf Sci. 2018;439:468-74. http://doi.org/10.1016/j.apsusc.2018.01.034.

33. Jia H, Gao M, Liu Z. Effect of Ti and Nb on microstructure and properties of Fe based surfacing alloy. Transactions of The China Welding Institution. 2023;44(3):87-91.

34. Archard JF. Contact and rubbing of flat surfaces. J Appl Phys. 1953;24(8):981-8. http://doi.org/10.1063/1.1721448.

35. Zong L, Zhao Y, Long S, Guo N. Effect of Nb content on the microstructure and wear resistance of Fe-12Cr-x Nb-4C coatings prepared by plasma-transferred arc welding. Coatings. 2020;10(6):585. http://doi.org/10.3390/coatings10060585.

36. Sawamoto A, Ogi K, Matsuda K. Solidification structures of Fe-C-Cr-(V-Nb-W) alloys. Trans Am Foundrym Soc. 1986;94:403-16.

37. Huang SG, Liu RL, Li L, Van der Biest O, Vleugels J. NbC as grain growth inhibitor and carbide in WC–Co hardmetals. Int J Refract Hard Met. 2008;26(5):389-95. http://doi.org/10.1016/j.ijrmhm.2007.09.003.

38. Xu Z, Li D, Diao G, Wu M, Fraser D, Li J, et al. Effects of NbC addition on mechanical and tribological properties of AlCrFeNi medium-entropy alloy. Tribol Int. 2024;194:109486. http://doi.org/10.1016/j.triboint.2024.109486.

39. Yang J, Huang J, Fan D, Chen S. Microstructure and wear properties of Fe-6wt.% Cr-0.55 wt.% C-Xwt.% Nb laser cladding coating and the mechanism analysis. Mater Des. 2015;88:1031-41. http://doi.org/10.1016/j.matdes.2015.09.108.

40. Xiao JK, Tan H, Chen J, Martini A, Zhang C. Effect of carbon content on microstructure, hardness and wear resistance of CoCrFeMnNiCx high-entropy alloys. J Alloys Compd. 2020;847:156533. http://doi.org/10.1016/j.jallcom.2020.156533.

41. Bourithis L, Papadimitriou GD. The effect of microstructure and wear conditions on the wear resistance of steel metal matrix composites fabricated with PTA alloying technique. Wear. 2009;266(11-12):1155-64. http://doi.org/10.1016/j.wear.2009.03.032.